PCCP

ROYAL SOCIETY OF CHEMISTRY

PAPER

View Article Online
View Journal | View Issue

Cite this: *Phys. Chem. Chem. Phys.*, 2025, **27**, 15460

Computational study of PEDOT derivatives: reducing air stability to satisfy the self-doping criteria of transparent conjugated polymers†

Florian Regnier, [ab] Mario Leclerc *[b] and Jérôme Cornil *[a]

Received 14th April 2025,
Accepted 23rd June 2025

DOI: 10.1039/d5cp01414j

rsc.li/pccp

PEDOT has been one of the most extensively studied conjugated polymers due to its unique combination of good transparency and high electrical conductivity, making it a promising alternative to ITO electrodes. With the aim of designing more conducting and transparent chains, we provide here a state-of-the-art quantum-chemical (TD)-DFT analysis to investigate whether significant HOMO level destabilization and red-shifted optical absorption in the doped state can be achieved through simple derivatization schemes. We demonstrate that a copolymer featuring an alternation of an EDOT unit and a substituted thiophene ring can compete with PEDOT. Moreover, the calculations indicate that the exact layout of the substituents on the thiophene rings can tune the extent of delocalization of the charge carriers in the doped state, and by extension the charge transport properties.

1. Introduction

Over the past few decades, the field of organic electronics has emerged as a promising alternative to conventional inorganic devices and continues to generate significant interest both in academia and industry.[1–3] This field relies on the use of π-conjugated semiconducting materials such as small molecules, oligomers or polymers.[2–5] The latter combine the processability and mechanical properties of thermoplastics with electronic and optical properties similar to inorganic materials.[6,7] They offer, by extension, the possibility to develop flexible, lightweight and low-cost printed devices[8–10] such as organic solar cells (OSCs),[2,5,11,12] organic light-emitting diodes (OLEDs),[2,5,13] organic field-effect transistors (OFETs)[3,5,14] and (bio)sensors.[15–17] These specific properties make them attractive in many different niche applications not adapted for their inorganic counterparts such as in portable or wearable electronics[9,10,18] and building-integrated systems (*e.g.*, vertical panels and windows).[9,10,19,20]

Among the wide range of polymers in the field, poly(3,4-ethylenedioxythiophene), known as PEDOT, stands out for its capacity to form transparent and conductive electrodes *via* water deposition of a poly(3,4-ethylenedioxythiophene):poly(4-styrene sulfonate) blend (PEDOT:PSS).[21–23] Many commercialized formulations are widely used in the field of energy,[24–26] electronics[27–29] and biological applications.[30–32] These polythiophene derivatives are also regarded as good alternatives to replace expensive,[33–36] unsustainable,[33,34,37] and brittle[34,35,38] indium tin oxide (ITO) electrodes typically used in devices owing to their good compromise between transparency in the visible region ($\geq$80%)[35,36,39] and conductivity.[34] Although the conductivity of pristine PEDOT:PSS is typically around 1 S cm^{-1},[21,22,34,40] it can be remarkably pushed up to $\sim$4000 S cm^{-1} after sulfuric acid post-treatments,[33,34,41] hence reaching the conductivity range of the ITO-coated glass ($\sim$3000–6000 S cm^{-1}) and even exceeding the ITO conductivity on a polyethylene terephthalate (PET) substrate ($\sim$2000 S cm^{-1}).[34] This significant conductivity improvement has been attributed to a nanomorphology rearrangement in the PEDOT:PSS films (from a pristine core–shell grain structure[22,23,42,43] to a crystalline nanofibril structure), which is induced by the removal of the excess amount of a PSS dispersion agent.[41,43,44]

Secondary doping strategies such as the addition of additives (*e.g.*, co-solvents,[45–47] plasticizers,[48] ionic liquids,[49–51] surfactants,[52,53] acids,[40] nanocarbon materials,[54] *etc.*) to the aqueous PEDOT:PSS solution can also enhance conductivity.[42,43] These additives promote molecular conformation changes,[54,55] solvent/additive screening effects,[45,47] ion exchange,[51,52] or proton transfer,[40] which in turn lead to phase segregation and/or improved charge dynamics.[40,42–44] The design of novel PEDOT-compatible supporting (poly)electrolytes represents a promising approach to enhance device lifetime under real outdoor conditions, including exposure to ambient humidity conditions and continuous solar illumination. Indeed, hydrophobicity,[56] pH,[57,58] water resistance[57,59] and thermal stability (>150 °C)[21,56,60–62] can be

[a] *Laboratory for Chemistry of Novel Materials, University of Mons, B-7000, Mons, Belgium. E-mail: Jerome.Cornil@umons.ac.be*

[b] *Department of Chemistry, Laval University, Quebec, G1V A06, Canada*

† Electronic supplementary information (ESI) available. See DOI: https://doi.org/10.1039/d5cp01414j

tailored, while maintaining good transparency and relatively high conductivities (~80 to 250 S cm^{-1}) after secondary-doping treatments.[56,58,59,63] The PEDOT:(poly)anion alternatives offer an effective way to minimize device stability issues (*e.g.*, oxygen or water diffusion, interfacial metal ion diffusion, *etc.*)[64–69] typically eased by the hygroscopic and acidic nature (pH ~ 1–2)[44,64,70,71] of conventional PEDOT:PSS[43,57] and may even achieve higher electronic film conductivities due to the reduced average charge hopping distance.[44]

Polymers developed with the concept of ''self-doping'' (*i.e.*, with counterions attached covalently to the conjugated backbone) also show conductivities competitive with standard ITO electrodes. Since the first thiophene-based example of a water-soluble self-doped conducting polymer elaborated by Heeger *et al.* in 1987,[72–74] numerous efforts have been undertaken to improve the optical and electronic properties of these materials.[75–79] Recent studies have reported high conductivities between 1 and 1000 S cm^{-1} for sulfonated PEDOT derivatives[6,80] with transmittance at 550 nm comparable to that of the (ITO)-coated PET electrode ($T_{550} \approx 78\%$),[39,81] hence achieving the required characteristics for touch screens and OLED or OSC applications.[82] Although the p-type self-doping mechanism remains unclear, it is believed to involve an oxygen reduction reaction (ORR) under acidic aqueous conditions.[83,84] Indeed, upon acidification of the neopentyl sulfonate group into the corresponding sulfonic acid, the potential hydrogen (pH) of the solution decreases from ~8 to ~2.[80] Consequently, the standard reduction potential (E^0) of oxygen in water rises from 0.40 V to 1.23 V (at 25 °C, V *vs.* NHE), meaning that the oxidation power of oxygen is higher.[80] Under such conditions, an efficient self-doping process is only possible when macromolecules exhibit a HOMO energy level destabilized above their air stability threshold (*i.e.*, −5.0 or −5.2 eV).[6,85,86] The self-doped polymers eliminate the need for the insulating PSS polyelectrolytes in films and minimize the use of additional pre-treatments[40,87–89] or post-treatments[40,88,89] often required to obtain such high conductivities, while potentially reducing fabrication steps and costs.[40,89]

Although the conductivities and stabilities obtained for self-doped PEDOT homopolymer and copolymer derivatives are promising, the optical transparency in the visible region of these polymers should be improved to further motivate their use as transparent electrodes. While 100 nm-thick films of neutral chains typically have a maximum absorption located between 500 nm and 600 nm,[6] quite similar to dedoped PEDOT films,[21,90] their doped state covers a significant range of the visible region (>600 nm), making them consequently light blue. Moreover, thicker doped films[80] exhibit a sharp decrease in transmittance at higher wavelengths, unlike (ITO)-coated electrodes.[34,35,39,81]

In this context, the goal of the present work is to investigate at the theoretical level the actual impact of different derivatization schemes in order to make PEDOT chains easily (self-)dopable. The target is thus to raise the HOMO level of the polymers as high as possible compared to PEDOT,[6,85,91] in complete opposition to the current mainstream idea of lowering the HOMO level to increase their stability against oxygen.[85,86,92] A second objective of the design would be to shift the maximum absorption of neutral chains toward longer wavelengths in order to trigger a higher transparency in the doped state. To do so, different strategies can be employed including: (i) molecular design by tuning the conjugated backbone[93–99] or by addition of electron-donating or electron-withdrawing substituents;[93,94,97–101] (ii) alternation of electron-rich and electron-deficient π-conjugated units (D–A structures also called push–pull systems),[5,94,96,98,99] as successfully done in the field of organic solar cells to match the absorption with the solar emission spectrum; and (iii) stabilization of the quinoid resonance form in thiophene-based structures to reduce the bond-length alternation and hence the bandgap.[5,94,99,102–104] The central issue here is thus to predict quantitatively the impact of such derivatization schemes prior to synthesis, thus highlighting the need for quantum-chemical calculations. Since another key constrain for industrial applications is to keep the synthetic route simple, the first series of derivatives analysed introduces mesomeric donor substituents (OCOR, OH, and NH_2 that are known to destabilize the HOMO level)[105] on the ethylene units of PEDOT or expands the size of the saturated chain from 2 to 3 carbon atoms (PEDOT → ProDOT), see Fig. 1.

Due to the limited impact of such functionalization evidenced by the calculations (*vide infra*), we have next considered alternating copolymers formed by an EDOT unit and a thiophene unit substituted by a donor or an acceptor substituent (Fig. 2). Doing so, the HOMO level could be raised up by 0.50 eV compared to the neutral non-substituted P(EDOT-thiophene) copolymer, *i.e.*, leading to an energy level similar to that of the PEDOT homopolymer. The maximum absorption could also be red-shifted by 22 nm (0.12 eV) compared to P(EDOT-thiophene), yielding an optical signature equivalent to that of neutral PEDOT.

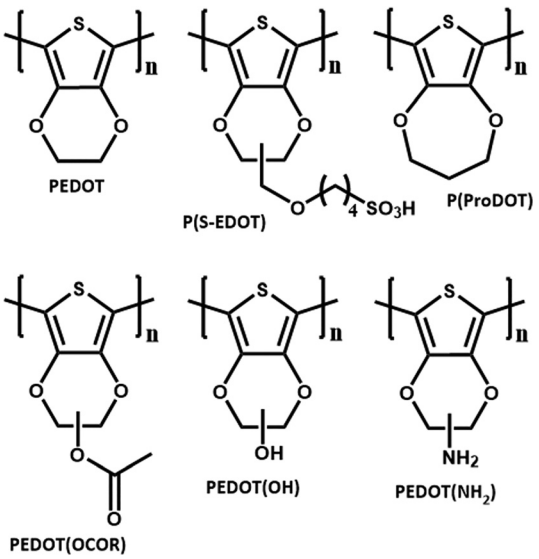

Fig. 1 Monomer unit considered in homopolymers.

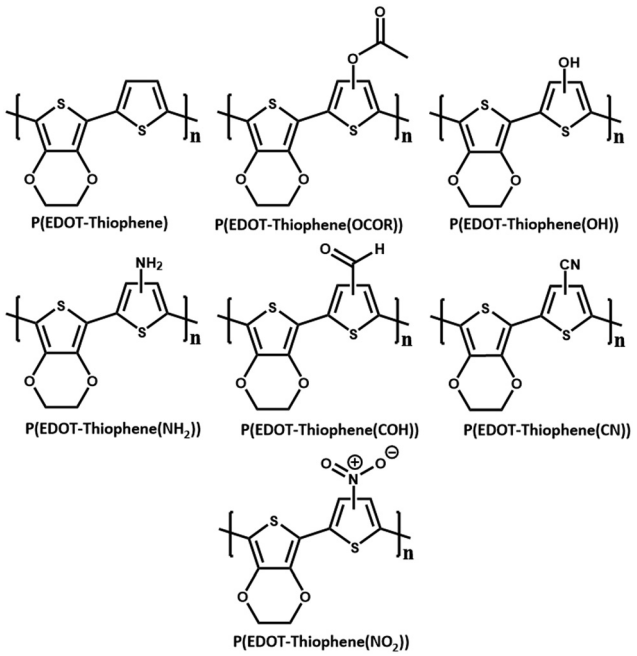

Fig. 2 Monomer unit considered in EDOT-based copolymers.

2. Theoretical considerations

2.1. Methodology

Kohn–Sham (KS) density functional theory (DFT) calculations have been carried out with the recommended Henderson version of the non-empirical long-range corrected hybrid exchange–correlation functional of Perdew–Burke–Ernzerhof (LC-ωHPBE),[106,107] with the 6-31G(d,p) basis set, as implemented in Gaussian 16 revision A.03 package.[108] The ω value has been optimally tuned for each system from the procedure described in the ESI† (S1). The closed-shell neutral systems are described within the restricted spin state formalism while the open-shell charged (*i.e.*, polaronic) systems are simulated within the unrestricted formalism that differentiates orbital energies and shapes for spin up (α) *versus* spin down (β).

Time-dependent (TD) DFT calculations with the same functional and basis set were carried out under vacuum by computing the lowest 100 excited states. The absorption spectra have been simulated with a full width at half-maximum (FWHM) set at 0.25 eV for all absorption bands. To provide a better description of each transition of interest, natural transition orbitals (NTOs) have been further computed at the same level of theory; they represent effective orbitals obtained by a weighted average of the different electronic excitations involved in the description of a given state.[109,110] These orbitals are plotted with an isovalue of 0.02. The overlap factor (ϕ_S) between the hole (ρ_h) and electron (ρ_e) density has also been estimated; this parameter varies from 0 for an excited state with a pronounced charge transfer characteristic (resulting in a very low intensity in the absorption spectra) to 1 for a very intense transition.[110]

In order to predict the optical properties of longer polymer chains not covered by the present calculations, a Kuhn fit has been performed from the transition energies calculated for oligomers of growing size.[111] This model initially developed for coupled resonators (in a linear chain and with alternating force constants k' and k_0) is able to depict how the energy of the lowest absorption band evolves with the number of monomer units (n) or the closely related number of double bonds (N_d) and in particular the saturation of the electronic and optical properties observed experimentally.[112–114] Since this model assumes that all units in the polymer are identical (*i.e.*, same geometry and charge), this fit is limited to the analysis of neutral systems and is written as[112,115]

$$E = E_0\sqrt{1 + 2\frac{k'}{k_0}\cos\frac{\pi}{N_d + 1}}$$

with E_0 (the vibrational energy of each resonator) and k'/k_0 being two adjustable parameters and N_d the largest number of conjugated double bonds along the shortest conjugated pathway in the oligomers.

The frontier orbital energies in the neutral polymer limit have also been estimated with the end-and-middle fragment Frontier orbital extrapolation tight binding-like model (EM-FFOE model)[116] and compared with a Kuhn fit. In the EM-FFOE model, Frontier molecular orbitals are viewed as a linear combination of the same type of orbital from each monomer unit, while assuming a coupling only between nearest-neighbour monomer orbitals. All monomer frontier orbitals are characterized by an isolated site energy (ε) and an intermonomer coupling energy between a terminal monomer unit and its neighbour (Δ_e) or an intermonomer coupling energy between two middle (non-terminal) monomers (Δ_m).[116] For an oligomer of n units, n-mer, the HOMO, LUMO and lowest energy transition ($S_0 \rightarrow S_1$ transition) are extrapolated with the following equations:

$$\varepsilon_{HOMO}(n) = \varepsilon + \frac{1}{2}\left(\Delta_m + \sqrt{\Delta_m{}^2 + 4\Delta_e{}^2}\right)$$

$$\varepsilon_{LUMO}(n) = \varepsilon_{S_0\rightarrow S_1} = \varepsilon - \frac{1}{2}\left(\Delta_m + \sqrt{\Delta_m{}^2 + 4\Delta_e{}^2}\right)$$

In the polymer limit ($n \rightarrow \infty$), these equations are reduced to $\varepsilon(\infty) = \varepsilon \pm 2\Delta_m$.

To depict the position of the positive charge in the charged systems, which is typically associated with a strong structural deformation of the chain due to the pronounced electron–phonon coupling,[103,117,118] bond length change (BLC) analysis has been carried out. Each point in a BLC distribution corresponds to the difference between a given bond length in the charged system and the length of the same bond in the neutral system. These analyses are complemented by an examination of the Mulliken charge differences (MCD) (*i.e.*, by plotting the charge of a given monomer unit in the charged system minus the charge of the same unit in the neutral system). To visualize the region of charge depletion *versus* charge accumulation, the electrostatic surface potential (ESP) profile of the most promising structures was calculated. We also estimated the hardness (η)[119,120] as half the difference between the adiabatic ionization

potential (IP) and electron affinity (EA). A high η value is indicative of a material with a high stability;[119,120] note that the values are here obtained in the gas phase and should be compared with other structures under the same conditions.

Since it is well established that the optoelectronic properties start to saturate between 8 and 10 repeated units,[94,113,115] accordingly, the major part of our analysis has been carried out on systems containing 8 or 9 thiophene-based units (for homopolymers and copolymers), which represents a good balance between the calculation time and accuracy. In copolymers, we define here a unit as an isolated thiophene block, that is, only one of the two comonomer blocks. Since there is no clear consensus on the choice of the terminal group (H ended or CH_3 ended unit), some calculations have been carried out on the 8-unit PEDOT for the two cases. The resulting HOMO energies show negligible differences (<0.1 eV)[121,122] for the neutral species, while the singly charged systems show larger differences up to 0.15 eV (S2, ESI†). Since methyl groups mimic the presence of inter-ring C–C linkages, such a termination was chosen for our study. In order to treat all systems on equal footing, the thiophene backbone of each polymer has been imposed to be planar, which is motivated by several factors including the high tendency of oligothiophenes and polythiophene chains to planarize in the condensed phase[113,123–128] and the core planarization effects induced in charged systems.[128,129] To further reduce the computing costs, the long alkyl chains typically linked to the conjugated backbone have been replaced by CH_3 groups[130,131] since saturated chains will not make a strong difference on the electronic and optical properties of isolated molecules[132–135] although we recognize that they play a major role in defining the chain packing.[93,132,135] Lastly, a C_i symmetry is imposed for each homopolymer as well as C_2 symmetry for copolymers to avoid the creation of non-symmetrical frontier orbitals when comparing the systems and to avoid deviations driven by localization effects, as clearly visualized with not constrained PEDOT(NH_2) and P(EDOT-thiophene(NH_2)) in the ESI† (S3). Details regarding the initial construction of all polymers analysed in this work can be found in Tables S1.1 and S1.2 in the ESI† (S4).

3. Results and discussion

3.1. PEDOT homopolymer and its derivatives

3.1.1. Neutral systems. The first systems analysed here are pristine PEDOT, sulfonated PEDOT (P(S-EDOT)), P(ProDOT) and other substituted derivatives (Fig. 1). The calculated shape of the HOMO and LUMO orbitals in the neutral 8-unit chain is presented in the ESI† (S5) and their relative energies are displayed in Fig. 3. Although these energies calculated in the gas phase cannot be considered in absolute values, their relative evolution is meaningful.[136]

Compared to the pristine PEDOT, P(S-EDOT) shows a small increase in the HOMO energy by 0.05 eV. P(ProDOT) stabilizes the HOMO level by 0.06 eV, while the esterified (OCOR), hydroxylated (OH) and aminated (NH_2) PEDOT chains stabilize

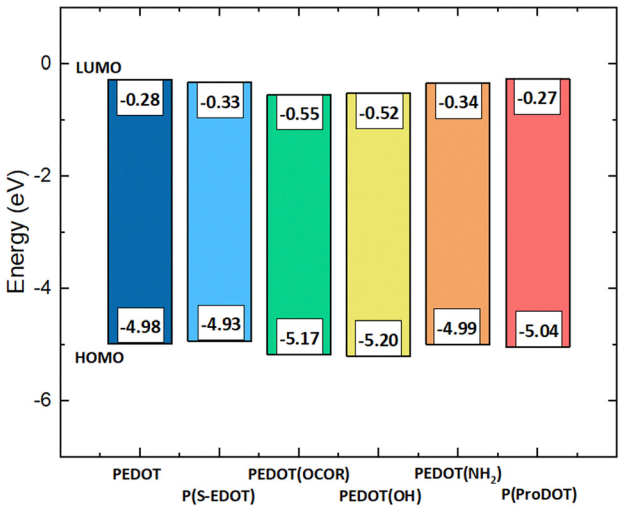

Fig. 3 Theoretical HOMO and LUMO energy values for 8-unit neutral homopolymer chains, as obtained at the DFT/LC-ωHPBE/6-31G(d,p) level.

the HOMO level by respectively 0.19 eV, 0.22 eV and 0.01 eV. This HOMO evolution that does not meet our requirements is thus driven by the electron-accepting inductive effects of the substituents, more pronounced for the oxygen atom due to its larger electronegativity. This motivates direct attachment of the substituents onto the conjugated core to activate in parallel the mesomeric effects (*vide infra*). The shapes of the frontier orbitals of all derivatives are similar to that of PEDOT (Fig. 4). No electronic density is found on the alkyl chains or on the electroactive substituent in the HOMO and the LUMO levels, pointing to the lack of π-electron delocalization between them and the central conjugated core.

The absorption spectra of the neutral homopolymers are displayed in Fig. 5. The optical signature of all compounds is quite similar except for P(ProDOT), which exhibits a small blue shift of 12 nm (0.07 eV) compared to PEDOT. This is

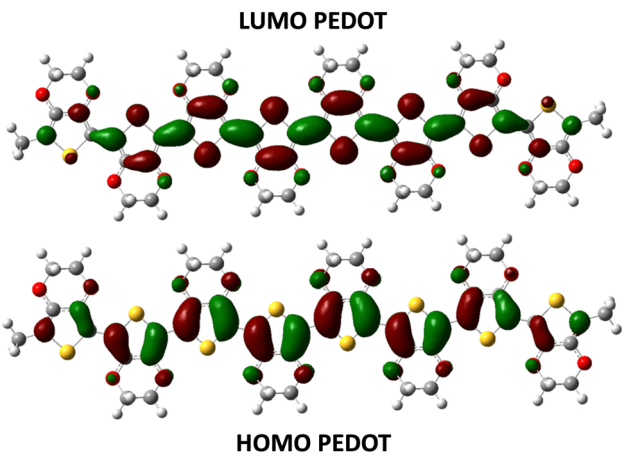

Fig. 4 Shape of the LUMO (upper figure) and HOMO (lower figure) orbitals in the 8-unit PEDOT polymer, as obtained at the DFT/LC-ωHPBE/6-31G(d,p) level. The wavefunction sign is represented by red (positive) and green (negative) colors.

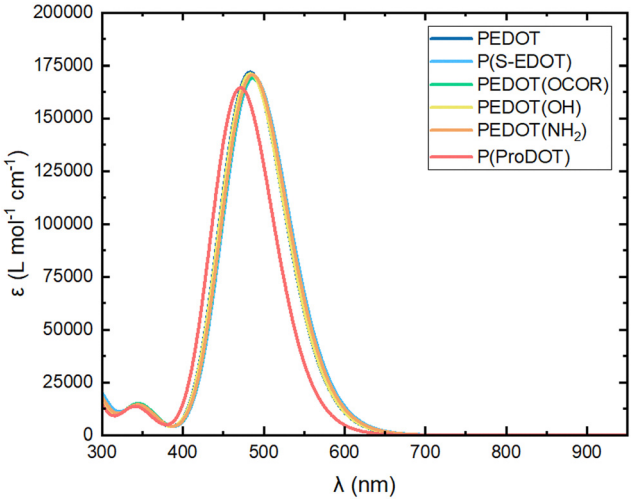

Fig. 5 Simulated optical absorption spectra for the neutral 8-unit homopolymer chains at the TD-DFT/LC-ωHPBE/6-31G(d,p) level.

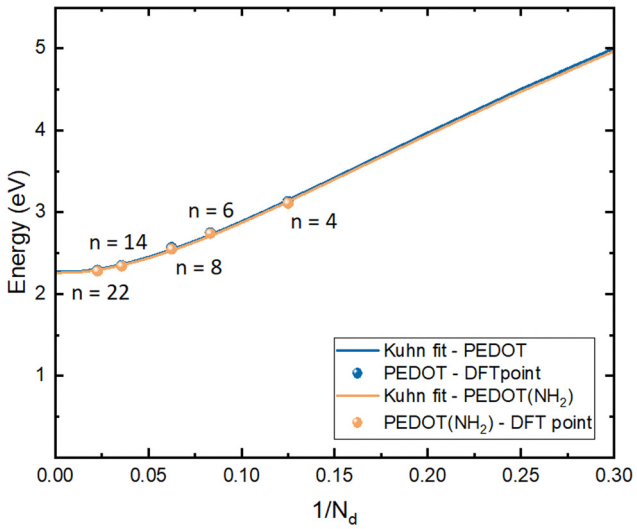

Fig. 6 Kuhn fit for PEDOT and PEDOT(NH_2) homopolymers. "N_d" corresponds to the number of double bonds and "n" stands for the number of units. All DFT points are obtained from TD-DFT/LC-ωHPBE/6-31G(d,p) computations.

rationalized by the fact that the inductive effects tend to shift symmetrically the frontier electronic levels mostly involved in the lowest absorption band. The maximum absorption (λ_{max}) for PEDOT, corresponding to the $S_0 \rightarrow S_1$ transition, is located at 483 nm (2.57 eV). The optical results obtained for the other neutral homopolymers can be found in Table S2 in the ESI.†

The shape of the NTOs associated with the $S_0 \rightarrow S_1$ absorption band and the relevant orbital contributions of the S_1 excited state (contribution value $\geq$2%) are presented in the ESI† (S6). As expected, the hole density (ρ_h) and electron density (ρ_e) display a very similar pattern compared to the corresponding frontier orbitals since this transition is primarily described by a HOMO→LUMO transition (~84%).[109] The overlap factor (ϕ_S) between the hole and electron density is systematically 0.83.

A Kuhn fit has been performed from $S_0 \rightarrow S_1$ optical transitions obtained for pristine PEDOT oligomers and PEDOT(NH_2) oligomers, the derivatives exhibiting the largest HOMO destabilization among the donor-substituted homopolymers. The estimated λ_{max} values for PEDOT and PEDOT(NH_2) of infinite length are 546 nm (2.27 eV) and 549 nm (2.26 eV), respectively (Fig. 6). Those predictions are in good agreement with the experimental spectra of neutral P(S-EDOT) thin films (λ_{max} ~ 530 nm)[6] but quite blue-shifted compared to the experimental spectra of high molecular weight P(S-EDOT) thin films (λ_{max} ~ 600 nm)[80] or PEDOT films (λ_{max} ~ 615 nm).[90] This small blueshift of about 0.2 eV could be reasonably attributed to solid-state aggregation effects as described by Spano's model of interacting molecules,[114,137–139] which is not taken into account in our computations. The optical properties start to saturate around 8 units (16 conjugated double bonds) and converge at 22 units (44 conjugated double bonds).[140] This trend can also be visualized from the evolution of the tuned ω parameter in the long-range corrected hybrid functional, which depends on the extent of electron delocalization,[141] see Table S3 in the ESI.†

The transition energies toward longer polymer chains have been extrapolated with the end-and-middle fragment Frontier orbital extrapolation (EM-FFOE) model.[116] Doing so for the PEDOT and PEDOT(NH_2) polymers (calculation details in S7, ESI†), the predicted λ_{max} values are respectively 546 nm (2.27 eV) and 549 nm (2.26 eV), in good accordance with the Kuhn fit. The EM-FFOE predicted HOMO energies for infinite homopolymers are respectively −4.66 eV and −4.74 eV. The electrostatic surface potential mapped onto the surface of the total electron density and the absolute hardness for 8-unit PEDOT and PEDOT(NH_2) are collected in the ESI† (S8).

3.1.2. Singly charged systems. Since PEDOT and its derivatives are intended to be used in their doped and conducting forms, prediction of the optical properties in their singly charged (*i.e.*, polaronic) states has been carried out. The optical signature of polaronic systems (Fig. 7) is the appearance of two subgap absorption features, as observed in many previous studies.[142–145] Typically, the lowest energy transition corresponds to the $S_0 \rightarrow S_1$ transition and is located around 1515 nm (~0.82 eV) in each compound, while the subgap feature associated with the $S_0 \rightarrow S_3$ transition lies around 740 nm (~1.68 eV). All absorption results can be found in Table S4 in the ESI.†

Since a singly charged chain is an open shell system, its electronic structure must be computed in an unrestricted formalism, implying that spin up and spin down can lie in orbitals with different shapes and energies. For the sake of illustration, Fig. 8 presents the two subgap transitions of a standard polaronic system. For the singly charged PEDOT, the $S_0 \rightarrow S_1$ transition is mainly described by the HOMO(β) → LUMO(β) transition (88%) while the $S_0 \rightarrow S_3$ transition mainly originates from the HOMO(α) → LUMO(α) transition (70%). The shape of the NTOs associated with these two features for each singly charged derivative and the relevant orbital

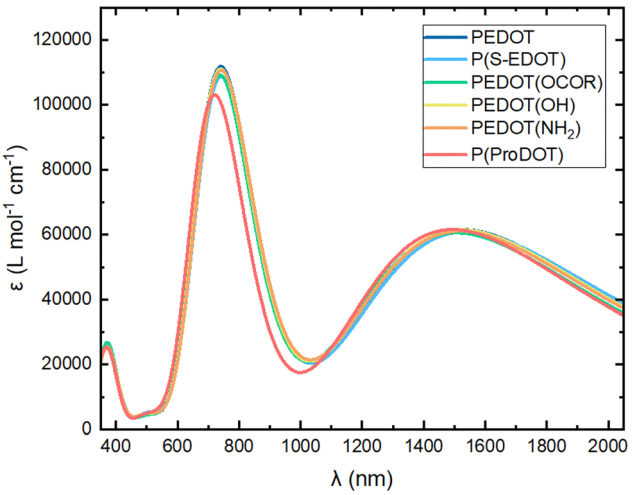

Fig. 7 Simulated optical absorption spectra of the singly charged 8-unit homopolymer chains at the TD-DFT/LC-ωHPBE/6-31G(d,p) level.

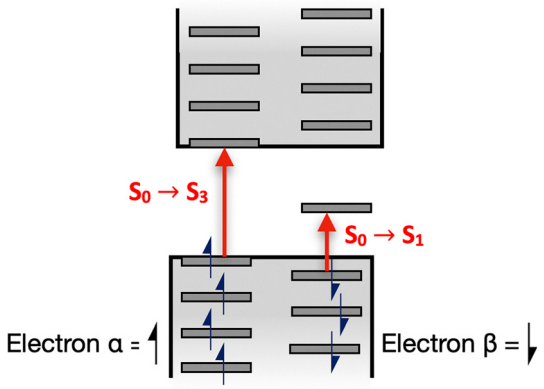

Fig. 8 Illustration of the origin of $S_0 \rightarrow S_1$ and $S_0 \rightarrow S_3$ transitions at the TD-DFT level for polaronic systems.

contributions of both excited states are presented in S9 (ESI†). The ϕ_S is around 0.82 for the $S_0 \rightarrow S_1$ transition and around 0.85 for the $S_0 \rightarrow S_3$ transition.

It is worth noting that the electronic structure sketched in Fig. 8 differs from the traditional picture featuring two electronic levels inside the bandgap;[128,145,146] the latter was actually inferred in the early days of the field of conducting polymers from calculations performed in the restricted formalism and is currently revisited in recent studies, primarily due to the controversial interpretation of ionisation potentials between neutral and charged systems and the need for considering the Hubbard U on-site interactions upon charging.[145,147,148]

The BLC distribution (Fig. 9-A) is identical for each homopolymer and shows pronounced structural modifications in the central units which decrease progressively when going towards the chain ends. To further support this description, Fig. 9-B shows the Mulliken charge differences (MCD) associated with each unit (unit no. 1 and no. 8 corresponding to the two terminal units). A Gaussian-like behaviour is found with 32% of the charge localized over the central two units (60% over the central four units). Note that the actual size might be affected by the presence of the counter-ion which is not included in the calculations.[149] The assignment of bond and unit numbers is shown in the ESI† in Fig. S10.

From all previous considerations, it is clear that the substitution patterns considered here for PEDOT decrease the HOMO energy level and do not change significantly the intrinsic optical properties of isolated chains. This is why another strategy has been explored which consists of using two different monomer blocks, *i.e.*, an EDOT unit and a substituted thiophene unit, to directly impact the core of the chains by both inductive and mesomeric effects induced by the substituent.[105] It is also worth stressing that such copolymers could offer in addition the possibility to introduce different side chains or electroactive groups for self-doping and solubilisation.

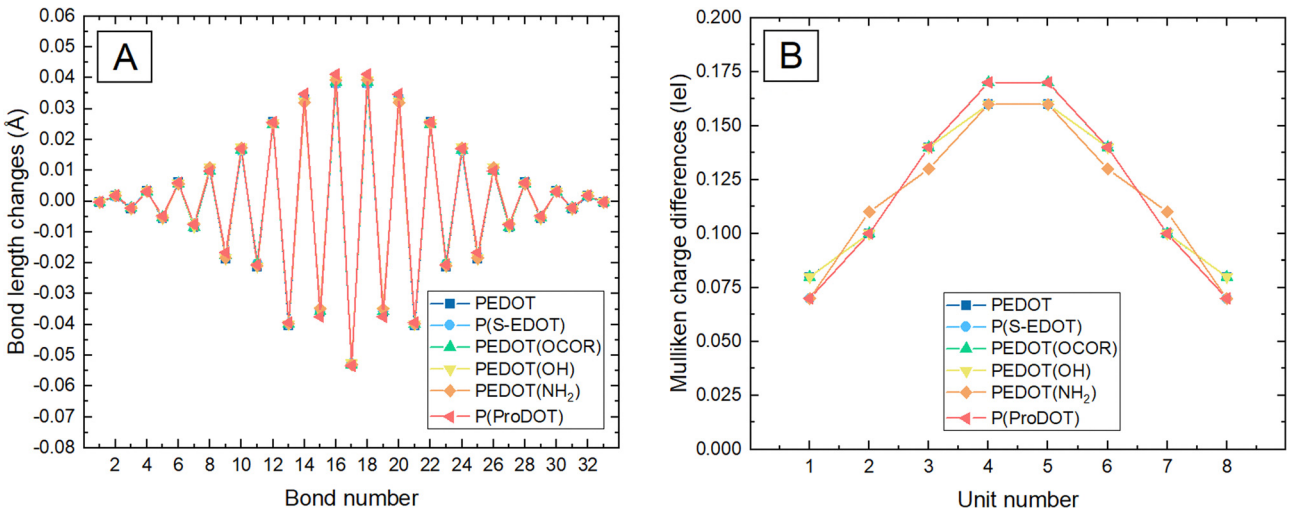

Fig. 9 BLC distribution (A) and MCD (B) analysis for the 8-unit PEDOT homopolymer and its derivatives.

3.2. P(EDOT-thiophene) copolymers

Due to the variable regioregularity levels of copolymers built from asymmetric monomers, modelling every possible structure of a single polymer chain would require immense computational costs and time. Moreover, to avoid the creation of asymmetrical frontier orbital distributions in our analysis and treat all systems on equal footing, as discussed previously, copolymers with 9 thiophene units and a C_2 symmetry must be considered here; attaching the substituents systematically on the same carbon site of the thiophene would indeed generate a strong net dipole that should be compensated by other chains in thin films, thus going beyond the scope of the present work. Due to the limited impact of the alkyl chains in P(S-EDOT) compared to PEDOT, as observed previously in computed homopolymers, the self-doping segments are completely neglected from the copolymer calculations to further minimise computational costs. As shown in Fig. 10, copolymers with a central EDOT unit can have 4 different substituent arrangements: (i) the L–R–L–R configuration (named here M1, with left (L) and right (R) being the side substitutions); (ii) the R–L–R–L configuration (named M2); (iii) the R–R–L–L configuration (named M3); and (iv) the L–L–R–R configuration (named M4). Comparing these four configurations provides new insights about the influence of substitution patterns on the electronic properties of the modelized polymers. The substituent choice for the thiophene units includes the same mesomeric donor groups used in the homopolymer section (–OCOR, –OH, and $–NH_2$) and mesomeric acceptor groups (–COH, –CN, and $–NO_2$) to generate a large diversity of donor–acceptor copolymers, with all units accessible through organic synthesis.[150–154]

3.2.1. Neutral systems. When comparing the influence of donor substituents for the M1 configuration of P(EDOT-thiophene), taken as a reference, gradual HOMO destabilization can be observed with respect to the function of the donor strength of the substituent. Specifically, P(EDOT-thiophene(OCOR)), P(EDOT-thiophene(OH)) and P(EDOT-thiophene(NH_2)) increase the HOMO energy level by 0.08 eV, 0.27 eV and 0.35 eV (Fig. 11).

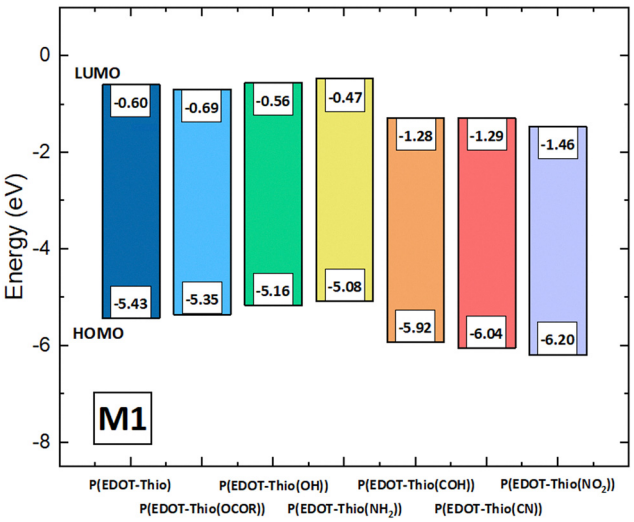

Fig. 11 Theoretical HOMO and LUMO energy level values for neutral 9-unit copolymers in the M1 configuration, as obtained at the DFT/LC-ωHPBE/6-31G(d,p) level. "Thio" is the abbreviation for "thiophene".

The same upward trend of the HOMO energy level can be seen in ESI† S11 and Table S5 for the M2 and M4 configurations. For the M3 configuration, the same trend is observed except for both OH and NH_2 derivatives which induce the same destabilization of the HOMO by 0.50 eV. For all results obtained for the four substitution patterns, see Table S5 in the ESI.†

Altogether, these results demonstrate that the HOMO energy level is slightly affected by the actual position of the ester group (0.02 eV), while larger deviations (up to 0.33 eV) are found with the hydroxyl and amino moieties. When compared to PEDOT-thiophene, the largest HOMO destabilization is obtained for the M3 systems with OH or NH_2 substituents (0.50 eV) and a HOMO very close to that of the 9-unit PEDOT homopolymer is obtained.

For systems substituted by the mesomeric acceptors, all 4 configurations show a downward trend in their HOMO energy level when compared to P(EDOT-thiophene). As shown in Fig. 11, the M1 series shows a decrease of the HOMO energy

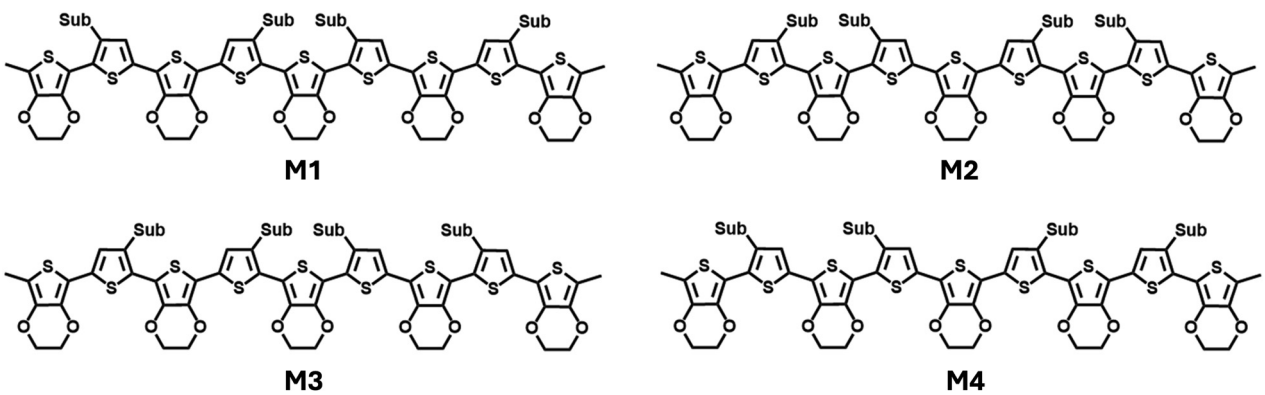

Fig. 10 Possible configurations in P(EDOT-thiophene) copolymer derivatives for the substitution layout on the thiophene units in (TD-)DFT computations. "Sub" stands for "substituent".

level of 0.49 eV, 0.61 eV and 0.77 eV for P(EDOT-thiophene(COH)), P(EDOT-thiophene(CN)) and P(EDOT-thiophene-(NO_2)), respectively. For all results obtained for the other series, see ESI† S11 and Table S6. Unlike the donor substituents, the comparison between the different M-systems shows more variations in their frontier orbital energy level stabilisation orders. Interestingly, the data in Table S6 (ESI†) suggest that only P(EDOT-thiophene(COH)) has a HOMO energy level strongly affected by the exact position of the electroactive substituents (up to 0.15 eV), while P(EDOT-thiophene(CN)) and P(EDOT-thiophene(NO_2)) show variations below 0.1 eV.

As shown in the ESI† (S12), analysing the spatial distribution of both frontier orbitals reveals that all copolymers present an electronic density over the thiophene substituents. In contrast to the PEDOT homopolymer and its derivatives described in the first section, this demonstrates the activation of the mesomeric effects of both the donor and acceptor substituents. When comparing the M1 configuration to the M4 configuration for any specific substituent, the shape of the HOMO varies as a function of the substitution pattern. This is particularly striking for the M3 series with donor groups which feature significant localization of the HOMO level.

In terms of optical properties, both donor and acceptor containing copolymers exhibit various variations in their spectral signatures compared to the P(EDOT-thiophene) reference, which has a calculated absorption maximum situated at 476 nm (2.61 eV). As shown in Fig. 12, the predicted spectra for all neutral M1 donor substituted systems show a bathochromic shift (red shift) of their λ_{max}: 489 nm (2.54 eV), 501 nm (2.47 eV) and 503 nm (2.47 eV) for P(EDOT-thiophene(OCOR)), P(EDOT-thiophene(NH_2)) and P(EDOT-thiophene(OH)), respectively, which fully parallels the corresponding trend of their electronic (HOMO–LUMO) gaps. Compared to 9-unit PEDOT (λ_{max} = 495 nm; 2.51 eV), all substituted polymers exhibit a similar signature without significant λ_{max} modification. A very similar trend is found for the other donor substitution patterns, see ESI† S13 and Table S7. The largest shift is in the order of 0.13 eV and is found with both hydroxyl and amino derivatives.

Since their interest became limited after the initial consideration of the HOMO energies, the optical absorption properties obtained for the copolymers with acceptor groups are gathered in the ESI† (S14), while their results are summarized in Table S8. The shape of the NTOs and the relevant orbital contributions associated with each lowest absorption band are presented in S15 (ESI†). ϕ_S is around 0.80 for the $S_0 \rightarrow S_1$ transition for all substituted M-systems.

From all the results above, it is clear that P(EDOT-thiophene(NH_2)) is the best copolymer candidate for increasing transparency and reaching the self-doping criteria. Indeed, this copolymer presents the highest HOMO level destabilization (up to 0.50 eV), while exhibiting a red-shifted absorption (0.12 eV) compared to unsubstituted P(EDOT-thiophene). These properties are actually quite comparable to those of pristine PEDOT.

The Kuhn fit for the P(EDOT-thiophene) and P(EDOT-thiophene(NH_2)) chains yielding the largest HOMO destabilization is plotted in Fig. 13. Doing so, P(EDOT-thiophene) and P(EDOT-thiophene(NH_2)) have a predicted λ_{max} of 521 nm (2.38 eV) and 549 nm (2.26 eV), respectively. Applying the EM-FFOE method to P(EDOT-thiophene) and P(EDOT-thiophene(NH_2)) results in respective λ_{max} values of 508 nm (2.44 eV) and 534 nm (2.32 eV), in very good quantitative agreement with the Kuhn fit. The HOMO energies predicted by the EM-FFOE model are −5.45 eV and −4.80 eV for P(EDOT-thiophene) and P(EDOT-thiophene(NH_2)) chains. Data used for the Kuhn fit and the EM-FFOE fit can be found in Tables S9 and S10 in the ESI,† while the EM-FFOE calculation details are presented in S16 (ESI†). The electrostatic surface potential mapped onto the surface of the total electron density and the absolute hardness for 9-unit P(EDOT-thiophene)

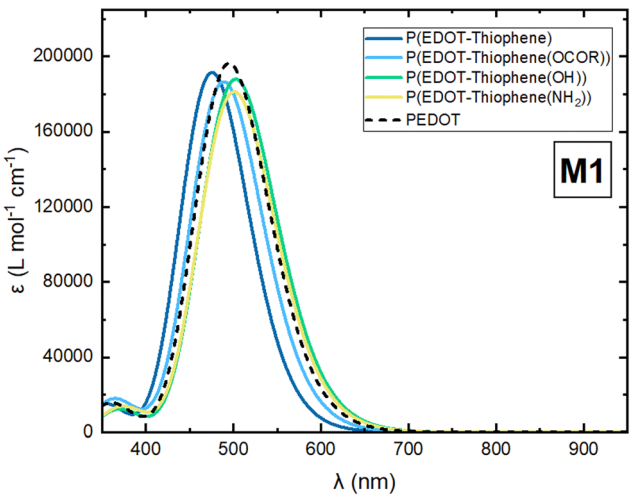

Fig. 12 Simulated absorption spectra for donor-containing 9-unit neutral copolymers in the M1 configuration, as obtained at the TD-DFT/LC-ωHPBE/6-31G(d,p) level.

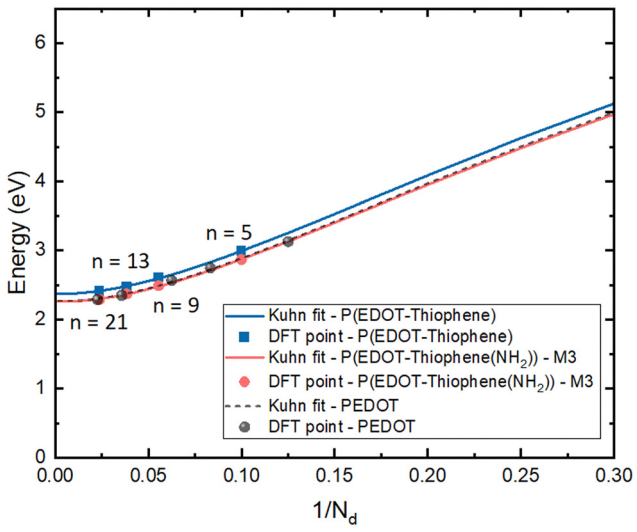

Fig. 13 Kuhn fit for P(EDOT-thiophene) and P(EDOT-thiophene(NH_2)) copolymers. "N_d" corresponds to the number of double bonds and "n" stands for the number of units. All DFT points are obtained from TD-DFT/LC-ωHPBE/6-31G(d,p) computations.

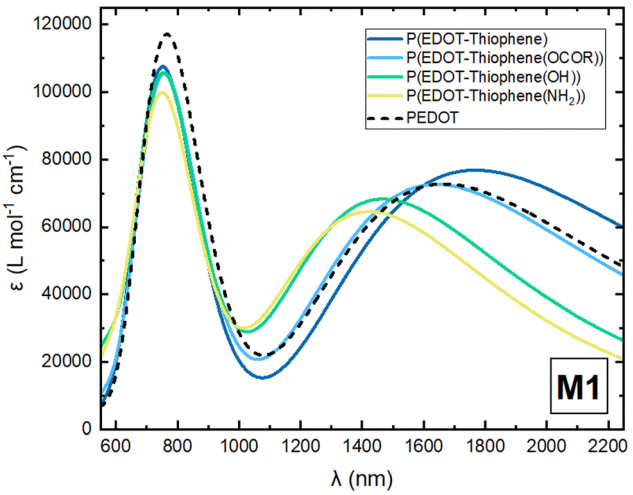

Fig. 14 Simulated absorption spectra for donor-containing 9-unit singly charged copolymers in the M1 system, as obtained at the TD-DFT/LC-ωHPBE/6-31G(d,p) level.

and P(EDOT-thiophene(NH_2)) in the M3 configuration are presented in the ESI† (S17).

3.2.2. Polaronic systems. Similar to the singly charged homopolymer systems previously analysed, the two subgap absorptions of polarons are presented for all studied copolymer systems. The 9-unit P(EDOT-thiophene) chain shows an $S_0 \rightarrow S_1$ transition located at 1768 nm (0.70 eV) and an $S_0 \rightarrow S_3$ transition at 755 nm (1.64 eV). In contrast to PEDOT derivatives that showed a minimal shift of the $S_0 \rightarrow S_1$ transition, the same transition in the copolymers varies as a function of the substituents. In donor substituted M1 systems (Fig. 14), this subgap transition exhibits a gradual hypsochromic shift (blue shift) as the mesomeric strength of the substituent increases: 1641 nm (0.76 eV), 1469 nm (0.84 eV) and 1425 nm (0.87 eV) for P(EDOT-thiophene(OCOR)), P(EDOT-thiophene(OH)) and P(EDOT-thiophene(NH_2)), respectively. The $S_0 \rightarrow S_3$ transition remains practically at the same energy for every system: 762 nm (1.63 eV), 756 nm (1.64 eV) and 758 nm (1.64 eV) within the same series.

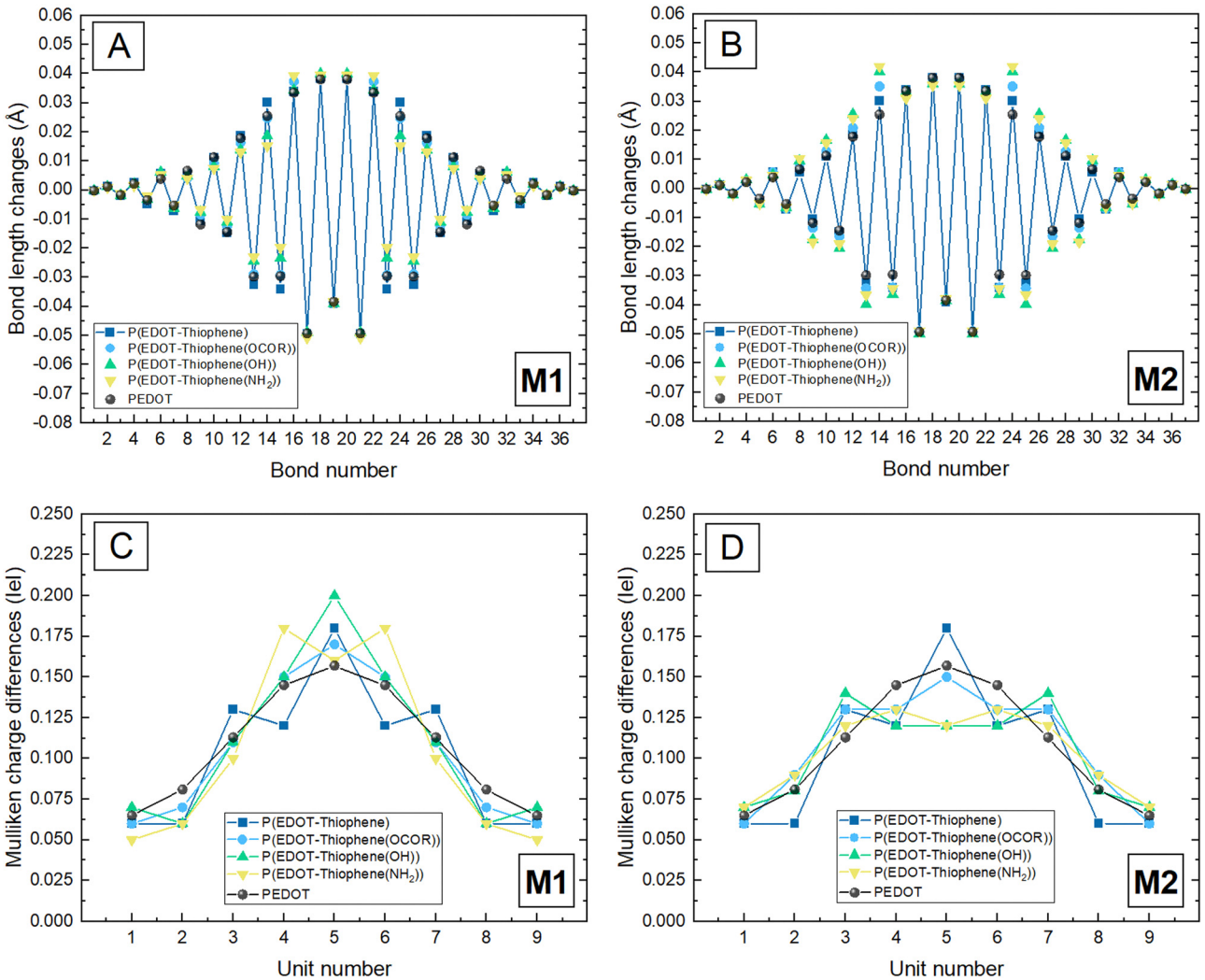

Fig. 15 BLC (A) and MCD distribution (C) for the 9-unit donor copolymers in the M1 system and BLC (B) and MCD distribution (D) for the 9-unit donor copolymers in the M2 system.

As seen in the ESI† (S18-B), the M2 donor substituted system shows a complete opposite trend for the $S_0 \rightarrow S_1$ transitions (red shift) when compared to M1: 1872 nm (0.66 eV), 1900 nm (0.65 eV) and 1987 nm (0.62 eV) for P(EDOT-thiophene(OCOR)), P(EDOT-thiophene(OH)) and P(EDOT-thiophene(NH_2)), respectively. The $S_0 \rightarrow S_3$ transition shows again small variations among the λ_{max} values: 776 nm (1.60 eV), 802 nm (1.55 eV) and 794 nm (1.56 eV) for the same series. All the results obtained for the M1 and M2 donor-containing copolymers suggest that the substitution pattern can have an impact on the charge distribution, and by extension on the optical properties. For all results obtained for the M1 and M2 systems, both substituted by mesomeric donor and acceptor groups, see S18 and Table S11 in the ESI.†

The NTOs associated with the $S_0 \rightarrow S_1$ transition in all M1 and M2 systems are presented in the ESI† (S19). The relevant orbital contributions associated with the $S_0 \rightarrow S_1$ transition are also presented. The hole density for each copolymer exhibits a modified distribution in the center compared to the neutral copolymers due to the presence of the positive charge. The ϕ_S for the $S_0 \rightarrow S_1$ transition is around 0.80 in M1 and around 0.84 in M2.

As for homopolymers in the first section, the copolymer analysis has been further supplemented by a BLC analysis coupled to an MCD analysis. As seen in Fig. 15-A, the BLC of all donor systems in the M1 configuration exhibits a pronounced variation in the center of the chains (from bond no. 16 to no. 22). A progressive decrease of the BLC is also observed when moving towards the chain ends. This decrease (from bond no. 15 to no. 1 and no. 23 to no. 37) is stronger for P(EDOT-thiophene(OH)) and P(EDOT-thiophene(NH_2)) than for P(EDOT-thiophene(OCOR)) and P(EDOT-thiophene). These observations point to a growing positive charge delocalization when going from NH_2 to OCOR derivatives. The charge in P(EDOT-thiophene(OH)) and P(EDOT-thiophene(NH_2)) is actually strongly confined between the two internal mesomeric groups (located between bond no. 15 and no. 16 and between bond no. 22 and no. 23), while the esterified derivative yields a more delocalized charge. By comparison with the optical spectra, the blue shift of the $S_0 \rightarrow S_1$ transition (from OCOR to NH_2) reflects a lower delocalization of the charge. The BLC distributions for the M2 donor substituted systems, presented in Fig. 15-B, exhibit a more extended structural deformation which is more pronounced for OH and NH_2 derivatives when moving towards the chain ends. These results point to a higher charge delocalization in P(EDOT-thiophene(OH)) and P(EDOT-thiophene(NH_2)) compared to P(EDOT-thiophene(OCOR)), which is found to translate into a red-shifted $S_0 \rightarrow S_1$ sub-band (from OCOR to NH_2) in their optical absorption spectra.

The charge (de)localization differences between M1 and M2 donor systems are also supported by MCD analysis that points to a strong charge localization in the central units in M1 (sharp peak in the distribution) and to a more pronounced charge delocalization in M2 (broad peak in the distribution), see Fig. 15-C and D. The assignment of bond and unit numbers is shown in the ESI† in Fig. S20. Additional analyses on acceptor copolymers in M1 and M2 configurations as well as on donor and acceptor copolymers in M3 and M4 configurations have been carried out to further investigate and confirm the relation between the charge (de)localization and the $S_0 \rightarrow S_1$ sub-band position, see S21, S22, S23 and S24 in the ESI.† The complete data set obtained for the M3 and M4 substitution patterns is collected in Table S12 in the ESI.† The NTOs and the relevant orbital contributions associated with the $S_0 \rightarrow S_1$ transition in M3 and M4 systems are presented in the ESI† (S25).

4. Conclusions

We have analysed by means of state-of-the-art quantum chemistry computations the impact of electroactive group substitution on the optical and electronic properties of EDOT-based polymers. The first part of our study has shown that the substitution of a PEDOT homopolymer with electron-donating groups on the ethylene bridge lowers the frontier orbital energies without strongly impacting the optical signature of the neutral and doped homopolymers, which did not meet our requirements to develop dopable and highly transparent polymers. These effects can be explained by the lack of mesomeric effects between the conjugated core and the substituents, which could have been triggered by hyperconjugation effects. We have next considered EDOT-containing copolymer derivatives introducing thiophene rings substituted by mesomeric donor groups (OCOR, OH, and NH_2) or mesomeric acceptor groups (COH, CN, and NO_2). The analysis of neutral systems shows large HOMO shifts compared to the P(EDOT-thiophene) chain attributed to mesomeric effects, strongly dependent on the nature of the electroactive groups and their relative position along the chain (M-systems). Among them, only OCOR, OH, and NH_2 groups destabilize the HOMO level. The most promising copolymer for achieving good transparency while meeting the prerequisites of the self-doping process is based on P(EDOT-thiophene(NH_2)) in the M3 configuration that yields a strong HOMO destabilization (0.50 eV) while yielding a red-shifted absorption band (0.12 eV) compared to P(EDOT-thiophene). This copolymer has properties very similar to those of PEDOT but offers in addition the possibility to introduce different side chains or electroactive groups for self-doping, optical bandgap modification and solubilisation. Interestingly, the energy of the lowest absorption band of the doped systems is found to be impacted by the positions of the electroactive groups along the polymer chain, which affects in turn the extent of charge (de)localization in the systems, as confirmed by the joint BLC and MCD analysis. Typically, a blue shift of the $S_0 \rightarrow S_1$ sub-band occurs upon charge localization whereas a red shift prevails when the charge gets delocalized. The copolymer structure is clearly an interesting starting point for further design towards improved optoelectronic properties compared to PEDOT.

Author contributions

Florian Regnier: conceptualization, investigation, methodology, writing – original draft, and writing – review & editing; Mario

Leclerc: conceptualization, funding acquisition, formal analysis, investigation, methodology, supervision, writing – original draft, and writing – review & editing; Jérôme Cornil: conceptualization, funding acquisition, formal analysis, investigation, methodology, supervision, writing – original draft, and writing – review & editing.

Conflicts of interest

There are no conflicts to declare.

Data availability

The input and output files of the calculations reported in this manuscript are available on demand from the corresponding author.

Acknowledgements

The work has been supported by the Fund for Scientific Research (FRS) of FNRS within the Consortium des Equipements de Calcul Intensif (CECI) under grant 2.5020.11, by the Walloon Region (ZENOBE Tier-1 supercomputer) under grant 1117545 and by the NSERC Green Electronics Network (GreEN) and Discovery Grants. J. C. is an FNRS research director.

Notes and references

1 N. Allard and M. Leclerc, *Functional Materials for Energy, Sustainable development and biomedical sciences*, De Gruyter, 2014, ch. 6, pp. 121–138.
2 Y. Shirota and H. Kageyama, *Handbook of organic materials for optical and (opto)electronic devices, Properties and applications*, Woodhead Publishing Limited, 2013, ch. 1, pp. 3–82.
3 S. R. Puniredd, W. Pisula and K. Müllen, *Handbook of organic materials for optical and (opto)electronic devices, Properties and applications*, Woodhead Publishing Limited, 2013, ch. 2, pp. 83–101.
4 J. C. Sancho-Garcia, *Handbook of organic materials for optical and (opto)electronic devices, Properties and applications*, Woodhead Publishing Limited, 2013, ch. 7, pp. 219–244.
5 M. P. Bracciale, C. Kim and A. Marrocchi, *Sustainable strategies in organic electronics*, Woodhead Publishing, 2022, ch. 1, pp. 3–71.
6 C. Beaumont, J. Turgeon, M. Idir, D. Neusser, R. Lapointe, S. Caron, W. Dupont, D. D'Astous, S. Shamsuddin, S. Hamza, E. Landry, S. Ludwigs and M. Leclerc, *Macromolecules*, 2021, **54**, 5464–5472.
7 S. C. Rasmussen, R. L. Schwiderski and M. E. Mulholland, *Chem. Commun.*, 2011, **47**, 11394–11410.
8 B. Lu, J. Wang, Z. Zhang, J. Wang, X. Yuan, Y. Ding, Y. Wang and Y. Yao, *Nano Sel.*, 2021, **2**, 2029–2039.
9 F. De Rossi, G. Polino and F. Brunetti, *Sustainable strategies in organic electronics*, Woodhead Publishing, 2022, ch. 13, pp. 463–503.
10 M. Riede, D. Spoltore and K. Leo, *Adv. Energy Mater.*, 2020, **11**, 2002653.
11 S. Guan, Y. Li, C. Xu, N. Yin, C. Xu, C. Wang, M. Wang, Y. Xu, Q. Chen, D. Wang, L. Zuo and H. Chen, *Adv. Mater.*, 2024, **36**, 2400342.
12 Q. Wei, W. Liu, M. Leclerc, J. Yuan, H. Chen and Y. Zou, *Sci. China: Chem.*, 2020, **63**, 1352–1366.
13 P. Petrova and R. Tomova, *Bulg. Chem. Commun.*, 2009, **41**, 211–225.
14 P. Mittal, S. Yadav and S. Negi, *Mater. Sci. Semicond. Process.*, 2021, **133**, 105975.
15 J. Borges-González, C. J. Kousseff and C. B. Nielsen, *J. Mater. Chem. C*, 2019, **7**, 1111–1130.
16 K. Potje-Kamloth, *Crit. Rev. Anal. Chem.*, 2002, **32**, 121–140.
17 G. C. Bazan and S. Wang, *Organic Semiconductors in Sensor Applications*, Springer, 2008, ch. 1, pp. 1–37.
18 X. Xu, Y. Zhao and Y. Liu, *Small*, 2023, **19**, 2206309.
19 L. D. Q. Corrêa, D. Bagnis, P. R. M. Franco, E. F. D. C. Junior and A. O. S. D. Costa, *Renewable Energy*, 2024, **220**, 119662.
20 H. M. Lee and J. H. Yoon, *Appl. Energy*, 2018, **225**, 1013–1021.
21 L. B. Groenendaal, F. Jonas, D. Freitag, H. Pielartzik and J. R. Reynolds, *Adv. Mater.*, 2000, **12**, 481–494.
22 Y. Yang, H. Deng and Q. Fu, *Mater. Chem. Front.*, 2020, **4**, 3130.
23 L. V. Kayser and D. J. Lipomi, *Adv. Mater.*, 2019, **31**, 1806133.
24 Q. Liu, Y. Jiang, K. Jin, J. Qin, J. Xu, W. Li, J. Xiong, J. Liu, Z. Xiao, K. Sun, S. Yang, X. Zhang and L. Ding, *Sci. Bull.*, 2020, **65**, 272–275.
25 S. G. Peera, K. K. Tintula, A. K. Sahu, S. Shanmugam, P. Sridhar and S. Pitchumani, *Electrochim. Acta*, 2013, **108**, 95–103.
26 S. Xu, M. Hong, X.-L. Shi, Y. Wang, L. Ge, Y. Bai, L. Wang, M. Dargusch, J. Zou and Z.-G. Chen, *Chem. Mater.*, 2019, **31**, 5238–5244.
27 P. Zhao, R. Zhang, Y. Tong, X. Zhao, T. Zhang, Q. Tang and Y. Liu, *ACS Appl. Mater. Interfaces*, 2020, **12**, 55083–55093.
28 Y. Guo, M. T. Otley, M. Li, X. Zhang, S. K. Sinha, G. M. Treich and G. A. Sotzing, *ACS Appl. Mater. Interfaces*, 2016, **8**, 26998–27005.
29 J. D. Ryan, D. A. Mengistie, R. Gabrielsson, A. Lund and C. Müller, *ACS Appl. Mater. Interfaces*, 2017, **9**, 9045–9050.
30 A. G. Guex, J. L. Puetzer, A. Armgarth, E. Littmann, E. Stavrinidou, E. P. Giannelis, G. G. Malliaras and M. M. Stevens, *Acta Biomater.*, 2017, **62**, 91–101.
31 B. Guo and P. X. Ma, *Biomacromolecules*, 2018, **19**, 1764–1782.
32 P. Sakunpongpitiporn, R. Morarad, W. Naeowong, S. Niamlang and A. Sirivat, *RSC Adv.*, 2024, **14**, 1549–1562.
33 O. Jianyong, *Acta Phys.-Chim. Sin.*, 2018, **34**, 1211–1220.
34 Z. Yu, Y. Xia, D. Du and J. Ouyang, *ACS Appl. Mater. Interfaces*, 2016, **8**, 11629–11638.

35 S. K. Hau, H.-L. Yip, J. Zou and A. K.-Y. Jen, *Org. Electron.*, 2009, **10**, 1401–1407.
36 C. J. M. Emmott, A. Urbina and J. Nelson, *Sol. Energy Mater. Sol. Cells*, 2012, **97**, 14–21.
37 G. B. Haxel, J. B. Hedrick and G. J. Orris, Rare earth elements: critical resources for high technology, Fact Sheet 087-02, 2002, DOI: 10.3133/fs08702.
38 W. Zhao and M. Cakmak, *J. Soc. Inf. Disp.*, 2014, **22**, 260–266.
39 C. Y. Leong, S. S. Yap, G. L. Ong, T. S. Ong, S. L. Yap, Y. T. Chin, S. F. Lee, T. Y. Tou and C. H. Nee, *Nanotechnol. Rev.*, 2020, **9**, 1539–1549.
40 F. Wu, P. Li, K. Sun, Y. Zhou, W. Chen, J. Fu, M. Li, S. Lu, D. Wei, X. Tang, Z. Zang, L. Sun, X. Liu and J. Ouyang, *Adv. Electron. Mater.*, 2017, **3**, 1700047.
41 N. Kim, S. Kee, S. H. Lee, B. H. Lee, Y. H. Kahng, Y.-R. Jo, B.-J. Kim and K. Lee, *Adv. Mater.*, 2014, **26**, 2268–2272.
42 J. Ouyang, *Displays*, 2013, **34**, 423–436.
43 Y. Jiang, T. Liu and Y. Zhou, *Adv. Funct. Mater.*, 2020, **30**, 2006213.
44 X. Crispin, S. Marciniak, W. Osikowicz, G. Zotti, A. W. Denier van der Gon, F. Louwet, M. Fahlman, L. Groenendaal, F. De Schryver and W. R. Salaneck, *J. Polym. Sci., Part B: Polym. Phys.*, 2003, **41**, 2561–2583.
45 J. Y. Kim, J. H. Jung, D. E. Lee and J. Joo, *Synth. Met.*, 2002, **126**, 311–316.
46 S. K. M. Jönsson, J. Birgerson, X. Crispin, G. Greczynski, W. Osikowicz, A. W. Denier van der Gon, W. R. Salaneck and M. Fahlman, *Synth. Met.*, 2003, **139**, 1–10.
47 J. Ouyang, C.-W. Chu, F.-C. Chen, Q. Xu and Y. Yang, *Adv. Funct. Mater.*, 2005, **15**, 203–208.
48 L. A. A. Pettersson, S. Ghosh and O. Inganäs, *Org. Electron.*, 2002, **3**, 143–148.
49 M. Döbbelin, R. Marcilla, M. Salsamendi, C. Pozo-Gonzalo, P. M. Carrasco, J. A. Pomposo and D. Mecerreyes, *Chem. Mater.*, 2007, **19**, 2147–2149.
50 C. Badre, L. Marquant, A. M. Alsayed and L. A. Hough, *Adv. Funct. Mater.*, 2012, **22**, 2723–2727.
51 S. Kee, N. Kim, B. S. Kim, S. Park, Y. H. Jang, S. H. Lee, J. Kim, J. Kim, S. kwon and K. Lee, *Adv. Mater.*, 2016, **28**, 8625–8631.
52 B. Fan, X. Mei and J. Ouyang, *Macromolecules*, 2008, **41**, 5971–5973.
53 M. Vosgueritchian, D. J. Lipomi and Z. Bao, *Adv. Funct. Mater.*, 2012, **22**, 421–428.
54 X. Hu, L. Chen, Y. Zhang, Q. Hu, J. Yang and Y. Chen, *Chem. Mater.*, 2014, **26**, 6293–6302.
55 A. G. MacDiarmid and A. J. Epstein, *Synth. Met.*, 1995, **69**, 85–92.
56 W. Cho, S. Im, S. Kim, S. Kim and J. H. Kim, *Polymers*, 2016, **8**, 189.
57 W. Yu, K. Wang, B. Guo, X. Qiu, Y. Hao, J. Chang and Y. Li, *J. Power Sources*, 2017, **358**, 29–38.
58 A. I. Hofmann, W. T. T. Smaal, M. Mumtaz, D. Katsigiannopoulos, C. Brochon, F. Schütze, O. R. Hild, E. Cloutet and G. Hadziioannou, *Angew. Chem.*, 2015, **127**, 8626–8630.
59 H.-E. Yin, C.-F. Lee and W.-Y. Chiu, *Polymer*, 2011, **52**, 5065–5074.
60 B. Somboonsub, M. A. Invernale, S. Thongyai, P. Praserthdam, D. A. Scola and G. A. Sotzing, *Polymer*, 2010, **51**, 1231–1236.
61 R. Kiebooms, A. Aleshin, K. Hutchison, F. Wudl and A. Heeger, *Synth. Met.*, 1999, **101**, 436–437.
62 L. Stepien, A. Roch, R. Tkachov, B. Leupolt, L. Han, N. van Ngo and C. Leyens, *Synth. Met.*, 2017, **225**, 49–54.
63 A. I. Hofmann, D. Katsigiannopoulos, M. Mumtaz, I. Petsagkourakis, G. Pecastaings, G. Fleury, C. Schatz, E. Pavlopoulou, C. Brochon, G. Hadziioannou and E. Cloutet, *Macromolecules*, 2017, **50**, 1959–1969.
64 K. Kawano, R. Pacios, D. Poplavskyy, J. Nelson, D. D. C. Bradley and J. R. Durrant, *Sol. Energy Mater. Sol. Cells*, 2006, **90**, 3520–3530.
65 M. JØrgensen, K. Norrman and F. C. Krebs, *Sol. Energy Mater. Sol. Cells*, 2008, **92**, 686–714.
66 K. Norrman, M. V. Madsen, S. A. Gevorgyan and F. C. Krebs, *J. Am. Chem. Soc.*, 2010, **132**, 16883–16892.
67 M. JØrgensen, K. Norrman, S. A. Gevorgyan, T. Tromholt, B. Andreasen and F. C. Krebs, *Adv. Mater.*, 2012, **24**, 580–612.
68 D. Fan, R. Zhang, Y. Li, C. Shan, W. Li, Y. Wang, F. Xu, H. Fan, Z. Sun, X. Li, M. Zhao, A. K. K. Kyaw, G. Li, J. Wang and W. Huang, *Front. Chem.*, 2021, **9**, 746365.
69 M. Pitaro, J. S. Alonso, L. Di Mario, D. G. Romero, K. Tran, T. Zaharia, M. B. Johansson, E. M. J. Johansson and M. A. Loi, *J. Mater. Chem. A*, 2023, **11**, 11755–11766.
70 M. P. de Jong, L. J. van IJzendoorn and M. J. A. de Voigt, *Appl. Phys. Lett.*, 2000, **77**, 2255–2257.
71 K. W. Wong, H. L. Yip, Y. Luo, K. Y. Wong, W. M. Lau, K. H. Low, H. F. Chow, Z. Q. Gao, W. L. Yeung and C. C. Chang, *Appl. Phys. Lett.*, 2002, **80**, 2788–2790.
72 A. O. Patil, Y. Ikenoue, N. Basescu, N. Colaneri, J. Chen, F. Wudl and A. J. Heeger, *Synth. Met.*, 1987, **20**, 151–159.
73 Y. Ikenoue, N. Outani, A. O. Patil, F. Wudl and A. J. Heeger, *Synth. Met.*, 1989, **30**, 305–319.
74 M. S. Freund BS and B. A. Deore, *Self-Doped Conducting polymers*, John Wiley & Sons, 2007, ch. 1, pp. 1–74.
75 N. S. Sundaresan, S. Basak, M. Pomerantz and J. R. Reynolds, *J. Chem. Soc., Chem. Commun.*, 1987, 621–622.
76 J. Yue and A. J. Epstein, *J. Am. Chem. Soc.*, 1990, **112**, 2800–2801.
77 M. Chayer, K. Faïd and M. Leclerc, *Chem. Mater.*, 1997, **9**, 2902–2905.
78 G. Zotti, S. Zecchin, G. Schiavon and L. B. Groenendaal, *Macromol. Chem. Phys.*, 2002, **203**, 1958–1964.
79 H. Yano, K. Kudo, K. Marumo and H. Okuzaki, *Sci. Adv.*, 2019, **5**, eaav9492.
80 C. Beaumont, T. Lemieux, S. Aivali, M. H. Sangachin, A. Gasonoo, T. M. St-Pierre, M. Bélanger, S. Beaupré, G. C. Welch and M. Leclerc, *ACS Macro Lett.*, 2024, **13**, 1133–1138.
81 K.-S. Tseng and Y.-L. Lo, *Opt. Mater. Express*, 2014, **4**, 764–775.

82 M. Morales-Masis, S. De Wolf, R. Woods-Robinson, J. W. Ager and C. Ballif, *Adv. Electron. Mater.*, 2017, **3**, 1600529.
83 S. K. Singh, X. Crispin and I. V. Zozoulenko, *J. Phys. Chem. C*, 2017, **121**, 12270–12277.
84 E. Mitraka, M. Gryszel, M. Vagin, M. J. Jafari, A. Singh, M. Warczak, M. Mitrakas, M. Berggren, T. Ederth, I. Zozoulenko, X. Crispin and E. D. Glowacki, *Adv. Sustainable Syst.*, 2019, **3**, 1800110.
85 D. M. de Leeuw, M. M. J. Simenon, A. R. Brown and R. E. F. Einerhand, *Synth. Met.*, 1997, **87**, 53–59.
86 B. C. Thompson, Y.-G. Kim and J. R. Reynolds, *Macromolecules*, 2005, **38**, 5359–5362.
87 E. Dauzon, A. E. Mansour, M. R. Niazi, R. Munir, D.-M. Smilgies, X. Sallenave, C. Plesse, F. Goubard and A. Amassian, *ACS Appl. Mater. Interfaces*, 2019, **11**, 17570–17582.
88 Y. H. Kim, C. Sachse, M. L. Machala, C. May, L. Müller-Meskamp and K. Leo, *Adv. Funct. Mater.*, 2011, **21**, 1076–1081.
89 C. Wang, K. Sun, J. Fu, R. Chen, M. Li, Z. Zang, X. Liu, B. Li, H. Gong and J. Ouyang, *Adv. Sustainable Syst.*, 2018, **2**, 1800085.
90 G. Sonmez, *Chem. Commun.*, 2005, 5251–5259.
91 X. M. Hong, H. E. Katz, A. J. Lovinger, B.-C. Wang and K. Raghavachari, *Chem. Mater.*, 2001, **13**, 4686–4691.
92 I. V. Martynov, L. N. Inasaridze and P. A. Troshin, *ChemSusChem*, 2021, **14**, 1–9.
93 J. Wang, P. Xue, Y. Jiang, Y. Huo and X. Zhan, *Nat. Rev. Chem.*, 2022, **6**, 614–634.
94 L. Dou, Y. Liu, Z. Hong, G. Li and Y. Yang, *Chem. Rev.*, 2015, **115**, 12633–12665.
95 H. Wang, J. Cao, J. Yu, Z. Zhang, R. Geng, L. Yang and W. Tang, *J. Mater. Chem. A*, 2019, **7**, 4313–4333.
96 D. Li, X. Zhang, D. Liu and T. Wang, *J. Mater. Chem. A*, 2020, **8**, 15607–15619.
97 J. Zhao, C. Yao, M. U. Ali, J. Miao and H. Meng, *Mater. Chem. Front.*, 2020, **4**, 3487–3504.
98 S. Dey, *Small*, 2019, 1900134.
99 Y.-J. Cheng, S.-H. Yang and C.-S. Hsu, *Chem. Rev.*, 2009, **109**, 5868–5923.
100 J. Huang and G. Yu, *Chem. Mater.*, 2021, **33**, 1513–1539.
101 G. P. Kini, S. J. Jeon and D. K. Moon, *Adv. Mater.*, 2020, 1906175.
102 S. Rasmussen, *Encyclopedia of Polymeric Nanomaterials*, Springer, 2013, pp. 1155–1166.
103 P. Chandrasekhar, *Conducting Polymers, Fundamentals and Applications: A Practical Approach*, Springer, 1999, ch. 2, pp. 23–42.
104 D. Jacquemin and C. Adamo, *J. Chem. Theory Comput.*, 2011, **7**, 369–376.
105 J. Cornil, D. A. Dos Santos, D. Beljonne and J.-L. Brédas, *J. Phys. Chem.*, 1995, **99**, 5604–5611.
106 T. M. Henderson, A. F. Izmaylov, G. Scalmani and G. E. Scuseria, *J. Chem. Phys.*, 2009, **131**, 044108.
107 O. A. Vydrov and G. E. Scuseria, *J. Chem. Phys.*, 2006, **125**, 234109.
108 *Gaussian 16 Rev.A.03 Release Notes*, 2017. **https://gaussian.com/relnotes_a03/**.
109 C. Risko and J.-L. Brédas, *Multiscale Modelling of Organic and Hybrid Photovoltaics*, Springer, 2013, ch. 1, pp. 1–38.
110 G. Londi, R. Dilmurat, G. D'Avino, V. Lemaur, Y. Olivier and D. Beljonne, *Phys. Chem. Chem. Phys.*, 2019, **21**, 25023–25034.
111 W. Kuhn, *Helv. Chim. Acta*, 1948, **31**, 1780–1799.
112 M. Böckmann, T. Schemme, D. H. de Jong, C. Denz, A. Heuer and N. L. Doltsinis, *Phys. Chem. Chem. Phys.*, 2015, **17**, 28616.
113 D. Khlaifia, C. P. Ewels, F. Massuyeau, M. Chemek, E. Faulques, J.-L. Duvail and K. Alimi, *RSC Adv.*, 2016, **6**, 56174.
114 F. P. V. Koch, PhD Dissertation No 20912, ETH Zurich, 2013.
115 J. Gierschner, J. Cornil and H.-J. Egelhaaf, *Adv. Mater.*, 2007, **19**, 173–191.
116 R. E. Larsen, *J. Phys. Chem. C*, 2016, **120**, 9650–9660.
117 F.-C. Chen, *Encyclopedia of Modern Optics*, Elsevier, 2018, 2nd edn, pp. 220–231.
118 A. D. Scaccabarozzi, A. Basu, F. Aniés, J. Liu, O. Zapata-Arteaga, R. Warren, Y. Firdaus, M. I. Nugraha, Y. Lin, M. Campoy-Quiles, N. Koch, C. Müller, L. Tsetseris, M. Heeney and T. D. Anthopoulos, *Chem. Rev.*, 2022, **18**, 4420–4492.
119 Z.-Z. Sun, W.-L. Ding, S. Feng and X.-L. Peng, *Phys. Chem. Chem. Phys.*, 2020, **22**, 16359.
120 Z.-Z. Sun, Y. Li and X.-L. Xu, *Phys. Chem. Chem. Phys.*, 2024, **26**, 6817–6825.
121 A. D. Becke, *J. Chem. Phys.*, 1993, **98**, 5648–5652.
122 T. Yanai, D. P. Tew and N. C. Handy, *Chem. Phys. Lett.*, 2004, **393**, 51–57.
123 A. Casey, S. D. Dimitrov, P. Shakya-Tuladhar, Z. Fei, M. Nguyen, Y. Han, T. D. Anthopoulos, J. R. Durrant and M. Heeney, *Chem. Mater.*, 2016, **28**, 5110–5120.
124 S. Hayashi, *Mater. Adv.*, 2020, **1**, 632.
125 T. Yamamoto, M. Usui, H. Ootsuka, T. Iijima, H. Fukumoto, Y. Sakai, S. Aramaki, H. M. Yamamoto, T. Yagi, H. Tajima, T. Okada, T. Fukuda, A. Emoto, H. Ushijima, M. Hasegawa and H. Ohtsu, *Macromol. Chem. Phys.*, 2010, **211**, 2138–2147.
126 R. D. McCullough, *Adv. Mater.*, 1998, **10**, 93–116.
127 C. Taliani and L. M. Blinov, *Adv. Mater.*, 1996, **8**, 353–359.
128 U. Salzner, *J. Phys. Chem. A*, 2008, **112**, 5458–5466.
129 D. A. da S. Filho, V. Coropceanu, D. Fichou, N. E. Gruhn, T. G. Bill, J. Gierschner, J. Cornil and J.-L. Brédas, *Philos. Trans. R. Soc., A*, 2007, **365**, 1435–1452.
130 J. Yuan, Y. Zhang, L. Zhou, G. Zhang, H.-L. Yip, T.-K. Lau, X. Lu, C. Zhu, H. Peng, P. A. Johnson, M. Leclerc, Y. Cao, J. Ulanski, Y. Li and Y. Zou, *Joule*, 2019, **3**, 1140–1151.
131 Y. Cui, H. Yao, J. Zhang, T. Zhang, Y. Wang, L. Hong, K. Xian, B. Xu, S. Zhang, J. Peng, Z. Wei, F. Gao and J. Hou, *Nat. Commun.*, 2019, **10**, 2515.
132 S.-C. Lan, C.-K. Chang, Y.-H. Lu, S.-W. Lin, A. K.-Y. Jen and K.-H. Wei, *RSC Adv.*, 2015, **5**, 67718.
133 K. Jiang, Q. Wei, J. Y. L. Lai, Z. Peng, H. K. Kim, J. Yuan, L. Ye, H. Ade, Y. Zou and H. Yan, *Joule*, 2019, **3**, 3020–3033.

134 Z. Luo, R. Sun, C. Zhong, T. Liu, G. Zhang, Y. Zou, X. Jiao, J. Min and C. Yang, *Sci. China: Chem.*, 2020, **63**, 361–369.
135 W. Peng, J. Xiong, T. Chen, D. Zhao, J. Liu, N. Zhang, Y. Teng, J. Yu and W. Zhu, *RSC. Adv.*, 2024, **14**, 8081.
136 G. Zhang and C. B. Musgrave, *J. Phys. Chem. A*, 2007, **111**, 1554–1561.
137 K. Kreger, H.-W. Schmidt and R. Hildner, *Electron. Struct.*, 2021, **3**, 023001.
138 O. G. Reid, J. A. N. Malik, G. Latini, S. Dayal, N. Kopidakis, C. Silva, N. Stingelin and G. Rumbles, *J. Polym. Sci., Part B: Polym. Phys.*, 2012, **50**, 27–37.
139 R. Ghosh and F. C. Spano, *Acc. Chem. Res.*, 2020, **53**, 2201–2211.
140 U. Salzner, *J. Chem. Theory Comput.*, 2007, **3**, 1143–1157.
141 T. Körzdörfer and J.-L. Brédas, *Acc. Chem. Res.*, 2014, **47**, 3284–3291.
142 J. Guay, P. Kasai, A. Diaz, R. Wu, J. M. Tour and L. H. Dao, *Chem. Mat.*, 1992, **4**, 1097–1105.
143 J. Yamamoto and Y. Furukawa, *J. Phys. Chem. B*, 2015, **119**, 4788–4794.
144 N. Massonnet, A. Carella, O. Jaudouin, P. Rannou, G. Laval, C. Celle and J.-P. Simonato, *J. Mater. Chem. C*, 2014, **2**, 1278.
145 I. Zozoulenko, A. Singh, S. K. Singh, V. Gueskine, X. Crispin and M. Berggren, *ACS Appl. Polym. Mater.*, 2019, **1**, 83–94.
146 J. Cornil and J.-L. Brédas, *Adv. Mater.*, 1995, **7**, 295–297.
147 D. Lungwitz, S. Joy, A. E. Mansour, A. Opitz, C. Karunasena, H. Li, N. A. Panjwani, K. Moudgil, K. Tang, J. Behrends, S. Barlow, S. R. Marder, J.-L. Brédas, K. Graham, N. Koch and A. Kahn, *J. Phys. Chem. Lett.*, 2023, **14**, 5633–5640.
148 C. G. Tang, K. Hou and W. L. Leong, *Chem. Mater.*, 2024, **36**, 28–53.
149 A. Dkhissi, D. Beljonne, R. Lazzaroni, F. Louwet and B. Groenendaal, *Theor. Chem. Acc.*, 2008, **119**, 305–312.
150 G. A. Hunter and H. McNab, *New. J. Chem.*, 2010, **34**, 2558–2563.
151 J. Bora, M. Dutta, T. Chetia and B. Chetia, *J. Mol. Struct.*, 2025, **1319**, 139418.
152 S. Fantasia, J. Windisch and M. Scalone, *Adv. Synth. Catal.*, 2013, **355**, 627–631.
153 F.-P. Wu, J.-B. Peng, L.-S. Meng, X. Qi and X.-F. Wu, *ChemCatChem*, 2017, **9**, 3121–3124.
154 S. Enthaler, M. Weidauer and F. Schröder, *Tetrahedron Lett.*, 2012, **53**, 882–885.